Hyperspectral UAV-sensing for monitoring tailing ponds: Towards responsible resource repurposing

Hernan Flores, Bastian Reker, Marcin Pawlik, Benjamin Haske, Tobias Rudolph

Research Center of Post-Mining (FZN), Technische Hochschule Georg Agricola (THGA), Herner Straße 45, 44787 Bochum, Germany, hernan.flores@thga.de

Abstract

The interest in repurposing mine residues has substantially increased over the last decade as the mining industry endeavors to minimize environmental footprints and legacies. The industry also aims to meet the growing demand for critical raw materials (CRMs), especially those essential for technology, by considering mine waste as a potential supplementary secondary resource. As part of the ongoing mine water management perpetual tasks in the Ibbenbüren coalfield in Germany (closed in 2018), residual sludge material from the Gravenhorst sewage treatment plant is deposited in tailing deposition ponds in the nearby area. In this contribution, we use hyperspectral and thermal drone-borne sensing as a tool to monitor and characterize such mine water residual material. The results contribute to the semi-quantification of iron content and critical minerals associated with secondary iron by-products, which may be subject to secondary prospecting.

Keywords: Mine waste, hyperspectral imaging, remote sensing, unmanned aerial system, tailing ponds, post-mining

Introduction

The shift towards cleaner energy sources requires a substantial demand for minerals. According to estimates from the World Bank and the International Energy Agency, in order to achieve climate goals, mineral production may need to surge by nearly 500% by the year 2050 (Hund et al. 2020). These targets require the pursuit of increasingly diffuse and lower-grade deposits, which present emerging challenges for sustainable mine waste management. New projects and perspectives about the management of legacy, active, and future mine wastes are increasingly framed into circular economy concepts: minimize environmental impact and lower costs while creating new economic value through revalorization (Kinnunen and Kaksonen 2019; Tayebi-Khorami et al. 2019)

Earlier research has established the advantages of utilizing remote sensing data for diverse environmental monitoring applications. Specifically concerning mining residues, certain studies have showcased the viability of employing field and imaging spectroscopy to identify minerals containing metals as indicators of contamination in mining areas (Farrand and Harsanyi 1997; Ferrier 1999). Montero et al. 2005 studied the characteristics of waste rock associated with acid drainage for protecting water reservoirs, while Sares et al. 2004 focused on indirect pH estimations of an AMD-stream by identifying iron-bearing minerals precipitated on the stream bed. Hyperspectral sensors are currently employed across various spatial dimensions, determined by the platform used for data acquisition (e.g., satellite, airborne, or lab-scale sensing for detailed mineralogical analyses) (Booysen et al. 2020). This versatility has enabled spectral monitoring to be applied effectively in characterizing different types of mining waste. For instance, Flores et al. 2021 utilized drone monitoring to assess river water affected by acid mine drainage from waste piles in the Rio Tinto region. Laboratory-scale analyses of mine dumps have been conducted not only to visualize associated risks but also to quantify metals for economic benefit, leveraging multiple sensors (Benndorf et al. 2022; Flores and Möllerherm 2023). In this contribution, we focus on characterizing one specific type of mining-originated residue: tailing sludge

ponds. The recovery of critical raw materials (CRMs) from these residues presents an important opportunity to meet the current and future demand while simultaneously helping to offset the costly expenses associated with waste treatment. Consequently, we explore the application of hyperspectral and thermal drone-based sensing as a means to monitor and characterize residual mine water materials deposited in such tailing facilities. We present a methodology that combines hyperspectral visible-to-near infrared, thermal and ground validation analyses to provide high-resolution maps and semi-quantify the elemental composition of the permanent deposition sites. The results aid in the semi-quantification of iron content and critical minerals linked to secondary iron by-products, which may be subject to secondary prospecting.

Methods and materials

Test site

As part of the perpetual mine water management tasks of the Ibbenbüren coalfield in Germany (closed in 2018), water from the former Westfeld flows out of the Dickenberg tunnel mouth without pumping and from there to the Gravenhorst sewage treatment plant. After treatment processing, water is discharged into the Ems via the Hörsteler Aa and residual sludge into tailing ponds in the nearby area.

Previous studies have found that certain critical raw materials (Al, B, Li, Mg, Sr, and Zn) were detected in the mine water from the Dickenberger adit (West field), which flows out without pressure (Stemke and Wieber 2022). The mineral loads of the water to be discharged are reduced substantially (Hensel et al. 2020). After treatment at the main Gravenhorst facility in Püsselburen, the sewage sludge is deposited into final landfill sites (Fig. 1a). These sites are constantly monitored and regularly watered to prevent fine sediments from becoming airborne in neighboring communities. Therefore, the material was partially flooded to the north during the survey day.

Figure 1 *(a) Orthophoto of the Tailing facility at Ibbenbüren showing the UAS-borne hyperspectral scanned scene and sampling locations (red-starts). (b) Unmanned aerial system (BlackBird V2 Hyperspectral Sensor on board the DJI M300). (c) DJI Mavic 2 Enterprise Advanced Thermal drone. (d) Detail of in-situ Fe concentration measurement. (e) Detail of the area and the characteristic color of sewage sludge material. (f) Detail of field sampling acquisition (water and sediment)*

Unmanned Aerial Systems and Sensors

Hyperspectral, thermal data and photogrammetry acquisition was accomplished by means of Unmanned Aerial Systems (UAS) and lightweight optical sensors. The unmanned aerial systems are small aircrafts (e.g., multicopters). Commonly known as drones, this platforms belongs to the Remotely Piloted Aircraft Systems (RPAS), which have increased in use in the last decade for different remotely sensed geological data acquisition (Booysen et al. 2020). For the purpose of this study, two Unmanned Aerial Systems (UAS) were utilized. Firstly, the DJI Matrice M300 drone, equipped with four propellers, provided a stable platform for image acquisition (DJI, 2020). This multi-copter allowed sufficient integration time for the spectral imaging sensor. The BlackBird V2 from HAIP manufacturer (HAIP Solutions GmbH, 2022), mounted on the Matrice M300 (Fig. 1b), features two distinct sensors – a hyperspectral (HIS) sensor and a separate RGB camera for high-quality livestreaming on the remote controller. The hyperspectral sensor captures images at a native resolution of 540 × 540 pixels, featuring 100 spectral channels across the wavelength range from 500 nm to 1000 nm. Secondly, the DJI Mavic 2 Enterprise Advanced Thermal drone (Fig. 1c), with a flight duration of approximately 28 minutes. This drone is equipped with two cameras – an RGB camera with a ½" CMOS sensor boasting a resolution of 48MP and a thermal camera with an accuracy of ± 2" (DJI, 2021). Similar to the DJI P4 MS drone, a Real Time Kinematic (RTK) module is integrated for centimeter accurate georeferencing of the acquired images.

The main goal of hyperspectral remote sensing (also known as imaging spectrometry or imaging spectroscopy) is to measure quantitatively the components of the Earth System from calibrated (radiance, reflectance or emissivity) spectra acquired as images in many, narrow and contiguous spectral bands (van der Meer et al. 2012). Collected data results in a three-dimensional data-cube composed of a set of pixels (represented as vectors), containing the measurement corresponding to a specific wavelength (Benediktsson and Ghamisi 2015). This provides the opportunity to query a plottable spectral signature for each spatial position on a surface. A spectral imaging dataset is composed by three dimensions with at least one, even indistinct, value defining the measured signal intensity along at least two spatial and one spectral axis (Lorenz 2019).

Sampling strategy

Due to the difficult access to the site, and the muddy soil conditions of the tailing facility, three sediment samples were taken at the edge of the pond (with the tag GNx; location in Fig. 1a), trying to collect samples at different humidity levels within the deposit (dry, semi-wet and covered with water). For each sampling point, the following field methodology was applied:

1) Record the Global Satellite Navigation System (GNSS) coordinates of the sampling point.
2) Take a sediment sample (Fig. 1f).
3) Measure the physicochemical parameters of the water (pH, Temperature, Eh) and Fe concentration (only achieved for sample GN02).
4) Take a general photograph of the area and the specific sampling site.
5) Take a brief description of the visual aspect of the water and sediment (color and presence of organic matter in the site).

The measurement of milieu parameters was achieved with a multi-parameters portable meter (WTW ProfiLine Multi 3320). The mV measurement of the redox potential was corrected for temperature and adjusted to a potential relative to that of the standard hydrogen electrode (see Method (Nordstrom 1977)). The pH meter was calibrated using Hanna standard solutions (pH 4.01 and pH 7.01) and redox potential was checked using Hanna standard solutions (240 mV and 470 mV). The probes were placed directly into the water with gentle agitation, and the measurement was taken once the reading stabilized (Method 2550: Baird et al. 2017). Two reagents were added to the water sample. First, 0.5 g of white crystalline powder (solid organic acid, $C_6H_8O_6$) reagent was added to

a 5 mL sample and shaken gently. Afterward, five drops of reagent 2 (Sodium thioglycolate) were added, gently shaken until the color appeared, which took approximately 15 min (Figs. 1d, 2a).

Geochemical analyses

Elemental characterization of sediment samples were performed at the German Mining Museum laboratories using X-Ray Fluorescence (XRF). Samples have been 100 mg dried sample mixed with 5 mL aqua regia in closed Teflon beakers. Heated to approx. 110 °C for 1–2 days. Solution with residue made up to 100 mL with distilled water. Sample solution diluted 1:10 with 2% HCl, plus 1ppb In as internal standard. Measurement of trace elements with external calibration (SF-ICP-MS, ELEMENT XR, Thermo Fisher Scientific).

Results

Table 1 summarizes the results of water chemistry analyses conducted during field recognition. The water exhibits neutral pH values and low electrical conductivity (EC). Although the redox conditions are currently low at 277.5 mV, it's important to note that these conditions can be influenced by the oxidation rate of Fe^{2+} to Fe^{3+}, potentially leading to a rapid increase. The surface water over the tailing material undergoes a continuous cycle of drying, with fresh water recharge to prevent the spread of dried residue. Given that this study was conducted during the summer, the water tends to dry quickly, resulting in brief interactions with the sediment. Consequently, the iron concentration in the water is relatively low (0.25 mL/g) as depicted in Fig. 2a.

Table 1. *Water quality parameters*

Parameter	Value
pH	8.2
Eh (redox)	277,5 mV
Temperature	19.9 °C
EC	3.15 mS/cm
Fe Concentration	0.25 mg/L

The XRF results are presented in their oxide forms, with aluminum (Al_2O_3), iron (Fe_2O_3), calcium (CaO_2), magnesium (MgO_2), and manganese (MnO_2) identified as the predominant constituents in the bulk geochemistry of the samples. To enhance visualization, the fractions have been normalized to 100% using a weighted average. For the selected samples shown in Fig. 2b, the iron fraction stands out with the following weighted averages: GN01 (63.99 wt% avg. Fe_2O_3), GN02 (62.25 wt% avg. Fe_2O_3), and GN03 (60.71 wt% avg. Fe_2O_3). Notably, the highest iron content and metal concentrations are observed in the driest part of the pond, as illustrated by GN01 (refer to Fig. 1a).

Fig. 3a displays spectral curves depicting the characteristics of the tailing sludge material. The material exhibits homogeneity in spectral behavior, yet there is a subtle difference between the wet and dry states. Spectral analysis has unveiled distinctive absorption features in two regions, revealing shapes and wavelength positions associated with iron mineralogy. These features are attributed to charge transfer (ligand-to-metal charge transfer) transitions and crystal field effects (transitions of electrons from lower to higher energy states) (Flores et al. 2021). Hematite is notably characterized by a narrower absorption feature around 880 nm, while goethite exhibits a broader feature with wavelengths around 920 nm or greater (Leybourne et al. 2008). The crystal field absorption around 900 nm, associated with this feature, is also observed in the spectral curves of jarosite and schwertmannite. However, further distinction for schwertmannite is possible due to charge transfer shoulders around 650 nm, associated with the charge transfer of Fe3+ and Fe2+ (Hunt 1977). Schwertmannite lacks a known inflection point at 650 nm and displays a spectral peak at 738 nm (Crowley et al. 2003). Preliminary mapping products are illustrated in Fig. 3b–c. The first presents an RGB zoom view derived from the orthomosaic image. Secondly, an iron ratio

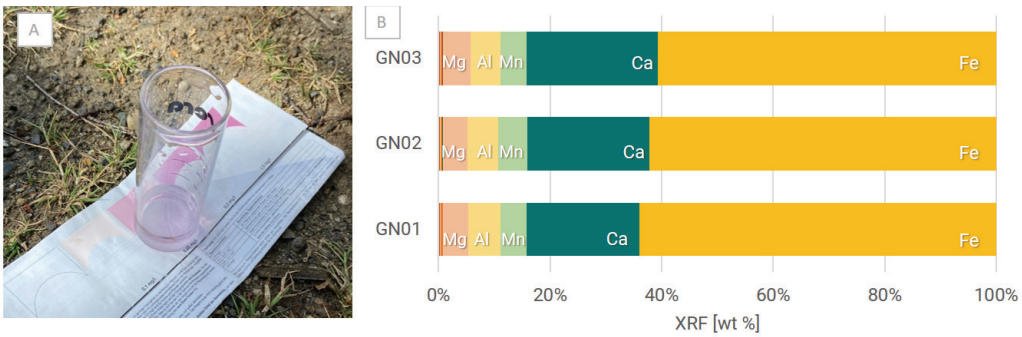

Figure 2 (a) In-situ Fe measurement on surface water. Color indicated 0.25 mL/g Fe concentration. (b) Chart of the main element fractions of three sludge samples determined by the XRF analysis

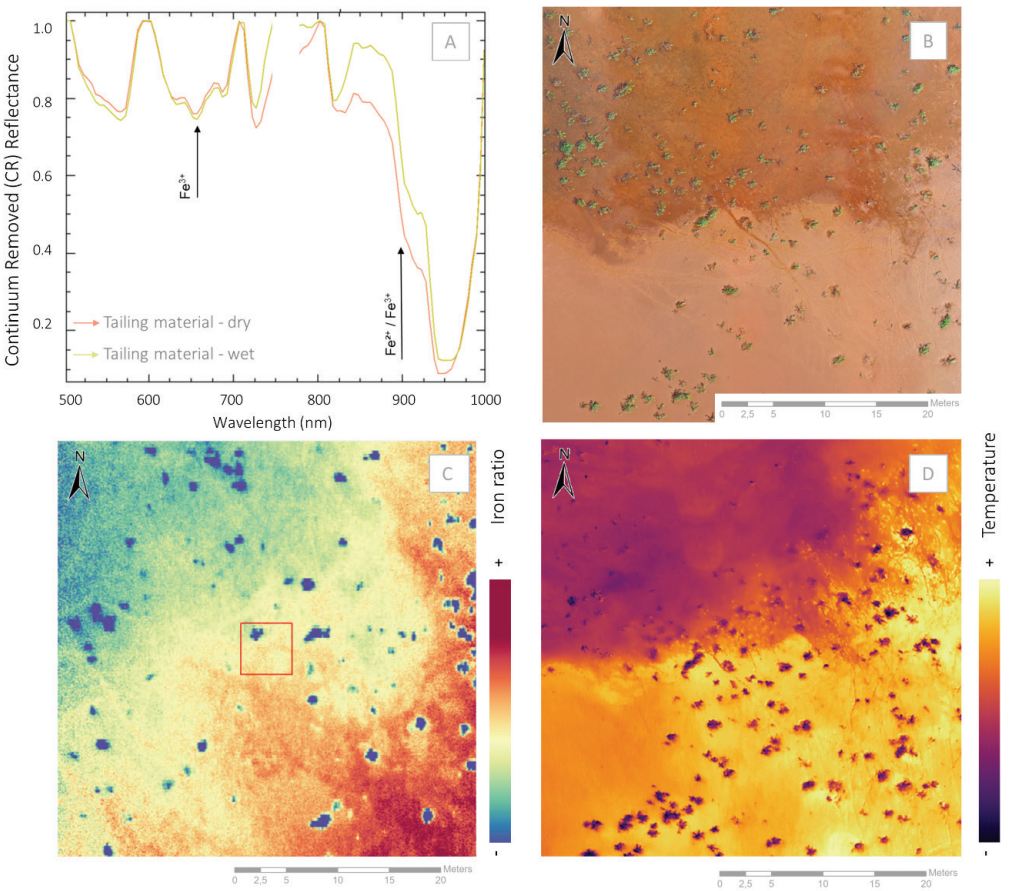

Figure 3 (a) Continuum Removal (CR) reflectance spectrum of the tailing sludge (dry and wet area). Black arrows indicate the absorption features at 650 nm and 900 nm. (b) RGB zoom. (c) Fe band ratio (650/735 nm) derived from hyperspectral scene. (d) Thermal orthophoto calculated from the captured thermal infrared data (Cropped to zoom)

has been calculated by combining bands 650/735 from the hyperspectral image to map the Fe absorption feature. As previously mentioned, the semi-quantification of iron may be influenced by surface water wetting the residual material. Notably, there is an observed increase in iron concentration towards the southern area (dry material), serving as a means to characterize the region. Thermal imaging further reveals the humid areas.

Conclusions

UAS-borne hyperspectral imaging serves as a fast and non-invasive tool, providing high-resolution maps for various environmental applications. We aim to characterize the tailing sludge material from the Ibbenbüren Gravenhorst treatment plant using two different sensors and state-of-the-art geochemical analysis, intending to achieve a holistic understanding of the material. The ultimate goal is to quantify metal concentrations and enhance their potential secondary prospectivity. The potential for revenue generation extends beyond the extraction of metals from tailing ponds to include the valorization of the bulk mineral fraction for various industrial applications (i.e. ceramics, bricks). Further digital processing routines that combine both datasets and utilize geochemical data as a training dataset are expected in the upcoming stages of the project.

Acknowledgments

The authors thank RAG AG Ibbenbüren for granting the access to the test site, the RAG Stiftung for funding the IAW33 project and the German Mining Museum, Dr. Michael Bode, and Mr. Till Genth for their assistance during the laboratory analyses.

References

Baird R, Eaton AD, Rice EW (12017) Standard methods for the examination of water and wastewater. American Public Health Association, Washington DC

Benediktsson JA, Ghamisi P (2015) Spectral-Spatial Classification of Hyperspectral Remote Sensing Images. Artech House

Benndorf J, Restrepo DA, Merkel N, et al (2022) TRIM4Post-Mining: Transition Information Modelling for Attractive Post-Mining LandscapesA Conceptual Framework. Mining 2:248–277. https://doi.org/10.3390/mining2020014

Booysen R, Gloaguen R, Lorenz S, et al (2020) Geological Remote Sensing. In: Reference Module in Earth Systems and Environmental Sciences, 2nd edn. Elsevier, pp 267–274

Crowley JK, Williams DE, Hammarstrom JM, et al (2003) Spectral reflectance properties (0.4-2.5 μm) of secondary Fe-oxide, Fe-hydroxide, and Fe-sulphate-hydrate minerals associated with sulphide-bearing mine wastes. Geochemistry: Exploration, Environment, Analysis 3:219–228. https://doi.org/10.1144/1467-7873/03-001

DJI (2020) User Manual MATRICE 300 RTK 2 Using This Manual Legends Warning Important Hints and Tips Reference Before Flight

Farrand WH, Harsanyi JC (1997) Mapping the distribution of mine tailings in the Coeur d'Alene River Valley, Idaho, through the use of a constrained energy minimization technique. Remote Sens Environ 59:64–76. https://doi.org/10.1016/S0034-4257(96)00080-6

Ferrier G (1999) Application of imaging spectrometer data in identifying environmental pollution caused by mining at Rodaquilar, Spain. Remote Sens Environ 68:125–137. https://doi.org/10.1016/S0034-4257(98)00105-9

Flores H, Lorenz S, Jackisch R, et al (2021) Uas-based hyperspectral environmental monitoring of acid mine drainage affected waters. Minerals 11:1–25. https://doi.org/10.3390/min11020182

Flores H, Möllerherm S (2023) TRIM4Post-Mining: Mine Waste Management and Risk Monitoring – A lignite mine case. 1–5. https://doi.org/10.3997/2214-4609.2023101158

HAIP SG (2022) PRODUCT DATA SHEET BLACK BIRD V2. Hannover

Hensel P, Kugel J, Terwelp T, Tuschmann J (2020) Long-Term Management of Mine Water Operations in the German Coalfields – an Interim Evaluation of the Findings Based on Operating Plans and Hydrological Permits Grubenwasserhaltung des Steinkohlenbergbaus für die Ewigkeit – Zwischenbilanz der Erkenntnisse. Mining Report Glückauf 156:97–105

Hunt GR (1977) Spectral Signatures of Particulate Minerals in the Visible and Near Infrared. Geophysics 42:501–513. https://doi.org/10.1190/1.1440721

Kinnunen PHM, Kaksonen AH (2019) Towards circular economy in mining: Opportunities and bottlenecks for tailings valorization. J Clean Prod 228:153–160. https://doi.org/10.1016/j.jclepro.2019.04.171

Leybourne MI, Pontual S, Peter JM (2008) Integrating Hyperspectral Mineralogy , Mineral Chemistry, Geochemistry and Geological Data at Different Scales in Iron Ore Mineral Exploration. 3:1–10

Lorenz S (2019) The Need for Accurate Pre-processing and Data Integration for the Application of Hyperspectral Imaging in Mineral Exploration

Montero IC, Brimhall GH, Alpers CN, Swayze GA (2005) Characterization of waste rock associated with acid drainage at the Penn Mine, California, by ground-based visible to short-wave infrared reflectance spectroscopy assisted by digital mapping. Chem Geol 215:453–472. https://doi.org/10.1016/j.chemgeo.2004.06.045

Nordstrom DK (1977) Thermochemical redox equilibria of ZoBells solution. Geochim Cosmochim 41:1835–1841. https://doi.org/10.1016/0016-7037(77)90215-0

Sares M, Hauff P, Peters D, Coulter D (2004) Characterizing Sources of Acid Rock Drainage and Resulting Water Quality Impacts Using Hyperspectral Remote Sensing–Examples from the Upper Arkansas. Advanced integration of geospatial technologies in mining reclamation, Dec 7–9, 2004, Atlanta, GA

Stemke M, Wieber G (2022) Closure of German Hard Coal Mines: Effects and Legal Aspects of Mine Flooding. Mine Water Environ 41:280–291. https://doi.org/10.1007/s10230-021-00842-7

SZ DJI Technology Co (2021) Mavic 2 Enterprise Series User Manual

Tayebi-Khorami M, Edraki M, Corder G, Golev A (2019) Re-thinking mining waste through an integrative. Minerals 9(5):286

van der Meer FD, van der Werff HMA, van Ruitenbeek FJA, et al (2012) Multi- and hyperspectral geologic remote sensing: A review. International Journal of Applied Earth Observation and Geoinformation 14:112–128. https://doi.org/10.1016/j.jag.2011.08.002